J Radioanal Nucl Chem (2016) 307:1231–1241
DOI 10.1007/s10967-015-4349-1

Synthesis of poly(acrylic acid–maleic acid)SiO_2/Al_2O_3 as novel composite material for cesium removal from acidic solutions

Mohamed F. Attallah[1] · K. F. Allan[1] · Mamdoh R. Mahmoud[1]

Received: 19 March 2015 / Published online: 1 August 2015

Abstract A novel composite material of SiO_2–Al_2O_3 based on poly(acrylic acid–maleic acid) was synthesized by irradiated with ^{60}Co γ-rays at a dose of 25 KGy. The composite material was characterized using FTIR, TGA and BET surface area. Adsorption of ^{134}Cs from HNO_3 was studied as a function of contact time, temperature and concentration of Cs. Sorption behavior of ^{134}Cs in different concentration of HCl, HNO_3, acetic acid, ascorbic acid, citric acid, NaCl and $NaNO_3$ solutions has been investigated. It can be concluded that the P(AA–MA)/SiO_2/Al_2O_3 is promising adsorbent for Cs removal from acidic liquid radioactive waste.

Keywords Cesium · Composite material · Kinetic model

Introduction

Radiocesium is a common constituent in radioactive wastewaters from nuclear processes. The availability of ^{137}Cs into environment poses a threat to the eco-system owing to its long life and unlimited solubility, which causes its migration to the biosphere through ground water and tends to remain in an available form to biota for several decades. Also, it is well known that radioactive cesium is an excellent gamma source for some clinical and biotechnological applications like surgical instrument disinfection, radiotherapy and food sterilization [1, 2]. Therefore, separation and recovery of radioactive cesium from waste solutions are a significant issue and has drawn particular attention of researchers. Hence, effective and simple methods should be explored for its removal before disposing of the wastes in aquatic systems.

From past few decades, considerable efforts have been directed towards the development of various physico-chemical methods for removal and recovery of radioactive Cs isotopes from nuclear waste streams involving co-precipitation, coagulation [3, 4], ion exchange [5–10], solvent extraction [11–15] and membrane processes [16–18].

Separation procedures based on adsorption phenomena are important in the analytical and radiochemistry of trace elements because of their simplicity, efficiency and selectivity. Fundamental investigations for better understanding of adsorption mechanisms of radionuclides will continue in order to be able to select most suitable materials for a particular requirement. Various types of inorganic and organic ion exchangers have been synthesized; however, inorganic ion exchangers generally are superior to organic resins because of their greater resistance to high temperature and high radiation, which is of great importance in the nuclear technology. In this regard, several types of adsorbents have been developed in recent years [19–27]. Insoluble metal oxides have attracted particular interest in the treatment of radioactive liquid wastes [19, 20]. These oxides are effective materials for the treatment of radioactive liquid wastes because they have an affinity for certain ions or groups of ions from both acidic and alkaline solutions.

Due to high amount inventory presences of radiocesium in acidic radioactive waste that produced during operation of different nuclear facilities, there has been increased attention by researchers [2, 12, 14, 16, 22, 28]. This attributed to challenge in order to find suitable efficient

✉ Mohamed F. Attallah
mohamedfathy_79@yahoo.com; dr.m.f.attallah@gmail.com

[1] Hot Laboratories and Waste Management Center, Atomic Energy Authority of Egypt, P.O. 13759, Abu Zaabal, Cairo, Egypt

materials for removal of radiounclides from acidic liquid radioactive waste. Ammonium molybdophosphate based on poly acrylonitrile (AMP-PAN) exhibits satisfactory sorption of cesium from acidic waste solution was reported by Raut et al. [22] and Tranter et al. [29]. Evaluation of resorcinol formaldehyde (RF) resin for removal of cesium from Hanford waste solutions was investigated by Hassan et al. [30]. Mrad et al. [31] investigated the preparation and characterization of zirconium phosphate (ZrP) in order to explore the behavior and the mechanism of radionuclide sorption onto amorphous, anhydrous crystalline and monohydrate crystalline phases of ZrP. The sorption of three radioisotopes ^{234}Th, ^{238}U, and ^{134}Cs from different concentrations of acidic solution (namely: nitric acid, hydrochloric acid and citric acid) onto three different phases of ZrP has also been reported.

The literature reports ^{137}Cs removal from alkaline nuclear waste using crystalline silicotitanates (CST) as exchange material [32]. Studies using CST from acidic waste feed [33, 34] have shown some success, but with less cesium adsorption capacity than is obtained with alkaline systems.

Crystalline silicotitanate manufactured and marketed by UOP as IONSIV IE-911 and an (AMP-PAN) composite sorbent have been evaluated for the removal of cesium from the Idaho National Engineering and Environmental Laboratory (INEEL) concentrated acidic tank waste has also been reported by Todd and Romanovskiy [35]. Spurred by need to find the suitable adsorbent materials with specific properties and looks essential to be utilized for treatment of acidic radioactive waste is still much attention. Therefore, the present work was carried out with a view to synthesize novel Al_2O_3–SiO_2 based on poly(maleic acid–acrylic acid) resin as novel composite material and evaluates their adsorption behavior of cesium from different acidic media. In order to understand the sorption mechanisms applicable for cesium sorption a number of kinetic models have been explored.

Experimental

Chemicals and reagents

All chemicals and reagents used in this study were of analytical grade and were used without further purification. Radioactive tracers ^{134}Cs (half-life 2.056 year) artificially produced in the 2nd Egyptian Nuclear Reactor, ERR-2, was finally used in the form of the corresponding nitrates.

Preparation of radio-tracer

For radiochemical investigations, radioactive tracer ^{134}Cs (half-life 2.06 years) was produced via irradiation of cesium chloride, at the Egyptian Second Research Reactor, ETRR-2. Accurately weighed portions of cesium chloride (about 10 mg) were wrapped in thin aluminum foils preliminary cleaned with acetone and were placed in thick aluminum irradiation capsules. These capsules were transferred to an aluminum irradiation of length 670 mm, arranged adjacent to the ETRR-2 core, and irradiated at a thermal neutron flux of 10^{14} n cm^{-2} s^{-1} for about 4 h.

Synthesis of composite polymeric material

Natural silicon and aluminum was obtained from natural material of bentonite that rich with Al and Si. A portion of bentonite was mixed with of sodium hydroxide and the ratio was kept at (1:1). The reaction was carried out at 600 °C for 2 h, then the mixture was dispersed in distilled water with stirring for 4 h. A co-monomer composition of acrylic acid–maleic acid (AA–MA) with 10 % for each monomer concentration was mixed with a constant portion of silicon/aluminum for the prepared composite materials as demonstrated in Table 1.

Each mixture was dissolved in de-oxygenated water the each mixture was stirred at room temperature for 2 h. The mixture was irradiated at dose 25 K Gy with the constant dose rate in gamma cell (^{60}Co). After irradiation the sample was filtrated from their aqueous solution. The samples were precipitated from their aqueous solution by adding excess acetone slowly with continuous stirring. Finally, the sample was dried in a vacuum at 50 °C overnight.

Characterization of composite polymeric material

Infrared absorption spectra

Infrared spectra of samples were measured by the standard KBr disc method using FTIR (Perkin Elmer Spectrum. The IR spectrum of P(MA–AA)–Al_2O_3–SiO_2 sample was scanned over the wave number range 600–4000 cm^{-1}.

Thermogravimetric analysis

Thermogravimetric analysis (TGA) and differential thermal analysis (DTA) of sample was performed at a heating rate of 15 °C min^{-1} using Shimadzu DTA-40 thermal analyzer.

Table 1 The concentration of co-monmer and inorganic in the irradiated composite material

Monmer		Si/Al (ml)	Dose rate (KGy/h)
AA (ml)	MA (ml)		
10	8	4	25

BET surface area

Characterizations of P(MA–AA)–Al_2O_3–SiO_2 sample was determined by nitrogen adsorption at −196 °C with the help of a Quantachrome Nova 1000e surface area and pore size analyzers. Before measurement, the sample was degassed at 300 °C for 2 h. The BET surface area, total pore volume and average pore radius were obtained from the adsorption isotherms.

Sorption experimental measurements

Batch experiments were conducted with 0.5–1.0 mm sieve size of composite polymeric material to investigate the effects of the contact time, temperature, and initial concentration of cesium as well as a different acidic solution on the sorption process.

The kinetic behavior of Cs was investigated by shaking 0.05 g of the prepared P(MA-AA)-Al_2O_3-SiO_2 with 5 mL of radioactive liquid waste containing 50 mg/L of Cs, at a speed of 300 RPM in thermostatic shaker at 298, 308, 318 and 328 K for a specified period of contact time. The clear liquid phase was obtained by filtration and the activity of ^{134}Cs in solution was determined radiometrically, using a high resolution (7.5 %) NaI(Tl) scintillation detector model 802-3X3, Canberra, USA. The distribution coefficient (K_d), removal percent (R %) as well as amount of metal ion sorbed onto the polymer at time (t), q_t (mg/g) were calculated from the following relations:

$$K_d = \frac{C_i - C_f}{C_f} \times \frac{V}{m} \text{ (mL/g)} \quad (1)$$

$$R(\%) = \frac{C_i - C_f}{C_i} \times 100 \quad (2)$$

$$q_t = \left(\frac{C_i - C_t}{C_i}\right) C_o \frac{V}{m} \text{ (mg/g)} \quad (3)$$

where C_i and C_t are the initial and the counting rate at time (t) per unit volume for the radionuclide, respectively; C_o is the initial concentration (mg/L) of metal ions used, V is the volume of the aqueous phase (mL), and m is the weight of the composite polymeric material (g).

Results and discussion

Characterization of composite polymeric material

FT-IR spectra

The FTIR Spectra of P(AA–MA) and P(AA–MA)SiO_2/Al_2O_3 composite and polymeric material, respectively, are shown in Fig. 1. The absorption peaks at 3419 and 3427 cm^{-1} are attributed to the stretching vibration of the hydroxide group (–OH) [36]. The slightly weak bands in the region 2925 and 2966 cm^{-1} are due to the stretching vibration of C–H groups. The peaks at 1719 and 1722 cm^{-1} indicates to C=O stretching vibration of carboxylic groups in the polymer and composite material. The peaks at 1428, 1167, 1104, 1074, 1036 cm^{-1} (in Fig. 1a) and 1429, 1172, 1102 and 1033 cm^{-1} (in Fig. 1b) are characterized for CH bending of the aliphatic –CH_2 groups [37]. The absorption bands at 902–506 cm^{-1} may be due to Si–O and Al–O bonds, this confirm the formation of composite material as shown in Fig. 1a. The absence of any absorption bands for C=C groups indicates the copolymerization of acrylic acid and malic acid.

Thermogravimetric analysis (TGA)

TGA and DTA thermograms of the prepared composite material are shown in Figs. 2. The TGA curve of the composite material showed a continuous loss in weight up to the maximum heating temperature used (600 °C). The TGA thermograph shows that the loss of weight occurs at different stages. In the first zone of the thermogram from 25–215 °C, the decrease of weight is 76.57 % for composite, which can be attributed to desorption of remaining water inside the crystal lattice of the composite. Within the temperature range from 215–500 °C the second weight loss reached to 17.61 %, which is corresponding to polymer decomposition [38]. This indicates that the thermal stability of polymer/oxide composites is superior to that of the pure polymer. It further demonstrates that the incorporation of SiO_2/Al_2O_3 improves the thermal stability of poly[-maleic acid-acrylic acid] by delaying the phase transformation process [39, 40].

DTA shows that endothermic peak at (59.1 and 136.4 °C) due to removal of external water molecules and endothermic peak at (195.8 °C) due to the removal of interstitial water molecules removed by condensation of –OH groups. The endothermic peaks at 219.6 and 256.3 °C as can be attributed to release of ammonia gas and CO_2 release as a result of dehydration of maleic acid [41].

Porous properties

The shape of the adsorption isotherm can provide qualitative information on the adsorption process and the extent of the surface area available to the adsorbate. The properties of the composite material were characterized in terms of pore volume and surface area. In order to determine the specific surface area and pore volume, composite was characterized by BET method. N_2 adsorption–desorption isotherms analysis of composite are shown in Fig. 3. As

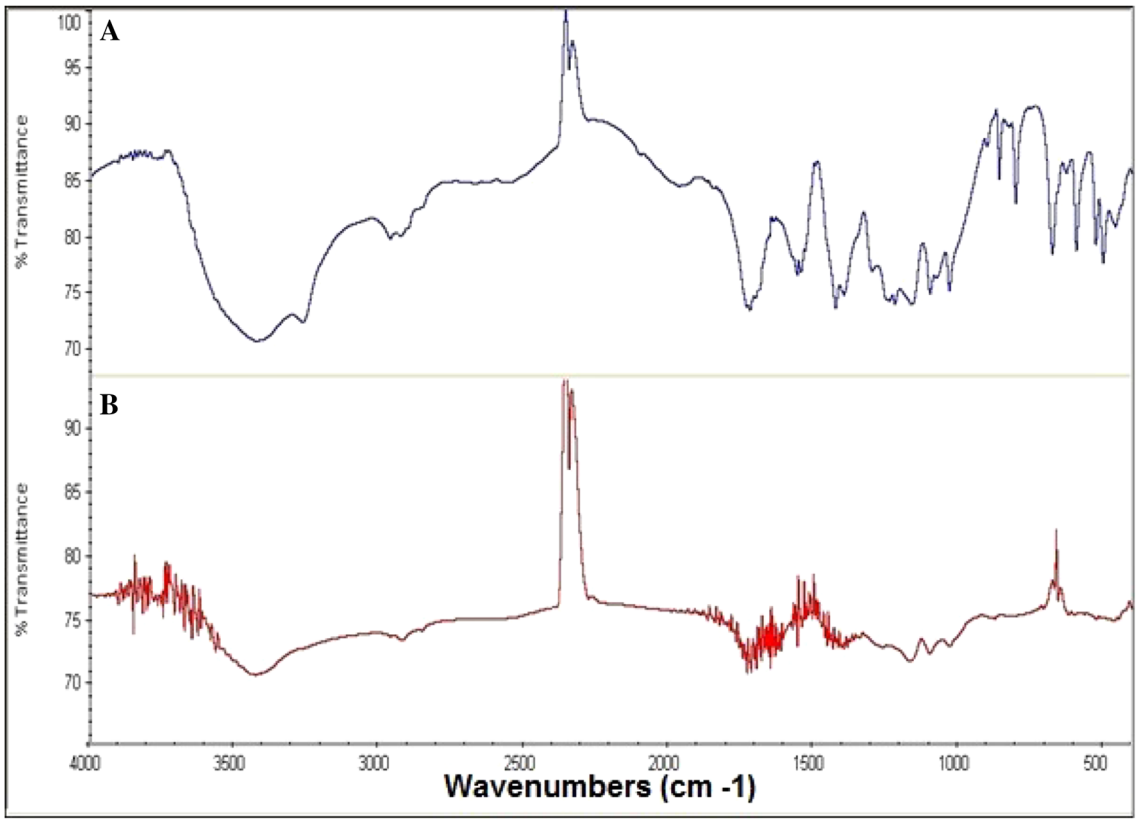

Fig. 1 FTIR spectra of (*1A*) P(MA–AM)SiO_2/Al_2O_3 (*1B*) P(MA–AA)

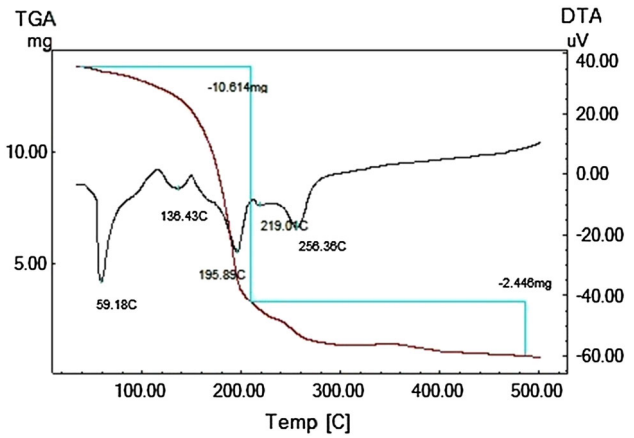

Fig. 2 TGA–DTA curves of P(AA–MA)SiO_2/Al_2O_3 composite material

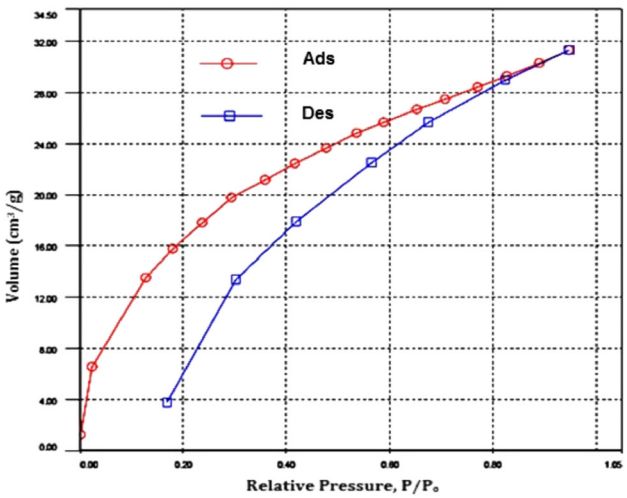

Fig. 3 Adsorption and desorption of N_2 by P(AA–MA)$/SiO_2/Al_2O_3$

shown in Fig. 3, the isotherm type of P(AA–MA)$/Al_2O_3$-SiO_2 is type IV according to the IUPAC isotherm, which is typical for mesoporous materials that exhibit capillary condensation and evaporation and that have large pore sizes with narrow size distributions. The pore characteristic of composite material is summarized in Table 2. The data obtained shows that BET surface area of the prepared composite is 67.74 m^2/g.

Adsorption behavior of ^{134}Cs

Adsorption of ^{134}Cs from different solutions

In order to determine the adsorptive properties of the Poly(AA–MA)$/Al_2O_3$–SiO_2 as a composite polymeric material used to separation of ^{134}Cs from different

Table 2 Porous structure parameters of poly(AA–MA)/Al_2O_3–SiO_2

Parameters	Values
BET-surface area (m^2/g)	67.74
Langmuir surface area (m^2/g)	133.8
Total pore volume (cm^3/g)	0.048
Average pore radius (nm)	1.429

solutions, such as hydrochloric acid, nitric acid, acetic acid, ascorbic acid, citric acid and sodium chloride as well as sodium nitrate solutions, has been investigated as listed in Table 3. It was found that the distribution coefficient of ^{134}Cs onto Poly(AA–MA)/Al_2O_3–SiO_2 is different according to the kind of solution. Under the same conditions, it was observed that the distribution coefficient of ^{134}Cs is decreased with increasing the concentration of hydrochloric acid, nitric acid, acetic acid, ascorbic acid, citric acid and sodium chloride as well as sodium nitrate solutions. The obtained results are in agreement with those reported in [5] for separation of Cs, Ba, Cu and Zn using zirconium antimonate (ZrSb) ion exchanger. It was also observed that the maximum removal of ^{134}Cs from HNO_3 and NaCl solutions has been obtained. This property is desirable in practical application. Therefore, the sorption potential, thermodynamic and kinetic behavior of P(AA–MA)/Al_2O_3–SiO_2 for the removal of ^{134}Cs from 0.1 M HNO_3 was further evaluated.

Effect of shaking time on adsorption of ^{134}Cs

Sorption is time-dependent process and the equilibrium times are one of the most important parameters for economical liquid waste treatment application. ^{134}Cs removal by P(AA–MA)/Al_2O_3–SiO_2 was studied using three different initial concentrations so as to optimize the adsorption equilibrium time. Figure 4 illustrates the adsorption of ^{134}Cs onto the P(AA–MA)/Al_2O_3–SiO_2 from 0.1 M HNO_3 aqueous solution as a function of contact time and initial concentration. It was found that the amount of ^{134}Cs adsorbed increases with increase in contact time, but after some time, it is gradually approaching a constant value, denoting attainment of equilibrium. The uptake of ^{134}Cs by P(AA–MA)/Al_2O_3–SiO_2 was very rapid at the beginning. The initial rapid phase may be due to the large number of vacant sites available at the initial period of the sorption. The amount of cesium adsorbed increases with time and reaches a constant value after about 2 h. After the equilibrium time, the amount of cesium adsorbed did not significantly change with time. This plateau represents saturation of the active sites available on P(AA–MA)/Al_2O_3–SiO_2 for interaction with cesium ions. It was assumed that the equilibrium time is that at which curves appear nearly asymptotic to the time axis. In the present case, the equilibrium time for ^{134}Cs removal was obtained at 120 min and hence considered for further study.

It can be seen that the adsorption of cesium at different concentrations is rapid in the initial stages and gradually decreases with the progress of adsorption until the equilibrium is reached. The amount of ^{134}Cs adsorbed at equilibrium (q_e) increased from 7.9 to 14.7 mg/g as the concentration was increased from 100 to 200 mg/l. This may be because an increase in the initial concentration enhances the interaction between cesium ions and the surface of P(AA–MA)/Al2O3–SiO2. The initial concentration of cesium provides an important driving force to overcome all mass transfer resistances of the cesium between the aqueous and solid phases. Hence a higher initial concentration of adsorbate will enhance the adsorption process. For higher initial concentration studied, it was found that there was no change in the equilibrium time at the observed initial cesium concentration range. The uptake of ^{134}Cs versus time curves is smooth and continuous leading to saturation, suggesting the possibility of monolayer coverage of cesium on the outer surface of P(AA–MA)/Al2O3–SiO2.

Adsorption capacity

The adsorption capacity of P(AA–MA)/Al2O3–SiO2 composite material for Cs was tested by measuring the q_e values of the radiotracer in the presence of various concentrations of the similar non-radioactive metal ion. The concentration of the non-radioactive metal ion was varied in the solution until maximum sorption capacity was obtained. As shown in Fig. 5, the highest sorption capacity of Cs (16 mg/g) for the composite material P(AA–MA)/Al_2O_3/SiO_2, from HNO_3 solution has been obtained. Low capacity is attributed to the inorganic portion of Al/Si reduced a number of functional groups and/or porous of P(AA-MA) which is known to be efficient for ion exchange/or adsorption of ions. Table 4 represents a comparison of the adsorption capacity of the P(AA–MA)/Al_2O_3/SiO_2 composite material with those other adsorbents reported from the literature for the adsorption of cesium. The obtained sorption capacity is relatively low compared with those stated in the literature.

Adsorption thermodynamic parameters

It is well known that temperature changes play an important role in the adsorption process [44–46]. To know an indication about thermodynamic of adsorption, the effect of temperature on the adsorption capacity should be studied. The plot of adsorption of ^{134}Cs as a function of temperature shows that adsorbed amount of ^{134}Cs decreased with temperature from 303 to 333 K, indicating that the adsorption is an exothermic process, as shown in Fig. 6. The temperature

Table 3 Distribution coefficient of ^{134}Cs onto P(AA–MA)/SiO_2/Al_2O_3 composite material from different media

Conc.	HCl	HNO_3	Acetic acid	Ascorbic acid	Citric acid	NaCl	$NaNO_3$
0.1	199.5	267	50	131	139	247	189
0.001	243	282	135	158	160	254	239
0.0001	250	322	170	171	201	384	265

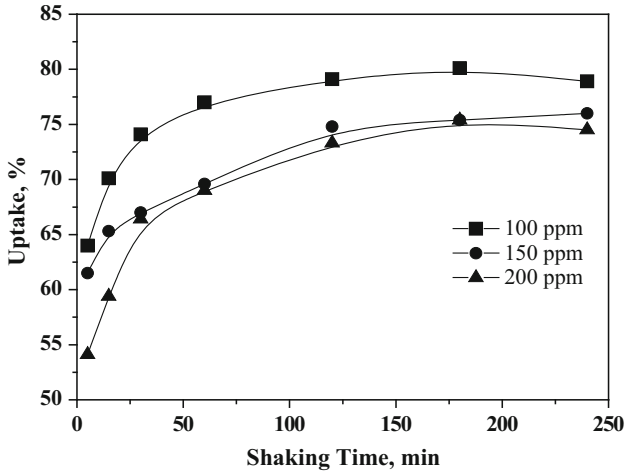

Fig. 4 Effect of contact time for removal of Cs from HNO_3 using P(AA–MA)SiO_2/Al_2O_3

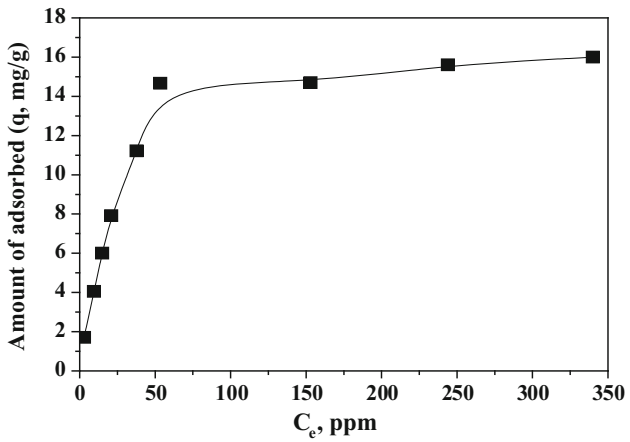

Fig. 5 Sorption capacity of ^{134}Cs onto P(AA–MA)SiO_2/Al_2O_3 from 0.1 M nitric acid solution

dependence of the adsorption process is associated with changes in several thermodynamic parameters. Thermodynamic parameters such as the change in free energy (ΔG), enthalpy (ΔH) and entropy (ΔS) of adsorption were calculated from the following equation [43, 44]:

$$\Delta G^{\circ} = -RT \ln K_c \quad (4)$$

where R is the gas constant (8.314 J/mol K), K_c is the equilibrium constant and T is temperature in K. The K_c value is calculated from Eq. (5):

$$K_c = \frac{C_{Ae}}{C_{Se}} \quad (5)$$

where C_{Ae} and C_{Se} is the equilibrium concentration of metal ions on adsorbent (mg/L) and in the solution (mg/L), respectively. Enthalpy (ΔH, kJ/mol) and entropy (ΔS, J/mol K) of adsorption can be estimated from van't Hoff equation as represented as follows:

$$\Delta G^{\circ} = \Delta H^{\circ} - T\Delta S^{\circ} \quad (6)$$

The van't Hoff plot for the adsorption of Cs onto the P(AA–MA)/Al_2O_3–SiO_2 was performed as a relation between ΔG° against T as shown in Fig. 7. The slope and intercept of the van't Hoff plot is equal to $-\Delta S$ and ΔH°, respectively. Thermodynamic parameters obtained are summarized in Table 5. The negative value of enthalpy change (ΔH) indicating the exothermic nature of the process that further confirms the experimental results, the entropy of adsorption (ΔS) reflects the affinity of the adsorbent material toward Cs and the negative free energy values ΔG indicate the feasibility of the process and its spontaneous nature [45].

Kinetic studies

Some kinetic models, namely, pseudo-first-order, pseudo second-order and intraparticle diffusion [8, 43, 44, 47] have been applied to the experimental data in order to analyze the sorption kinetics of ^{134}Cs onto the P(AA–MA)/Al_2O_3–SiO_2. The Mathematical equations of these models that have been tested the experimental data are described as follows:

Pseudo-first-order

$$\log (q_e - q_t) = \log q_e - \frac{k_1}{2.303} t \quad (7)$$

Pseudo-second-order

$$\frac{t}{q_t} = \frac{1}{k_2 q_e^2} + \frac{t}{q_e} \quad (8)$$

Intraparticle diffusion

$$q_t = k_{int} t^{0.5} + C \quad (9)$$

where q_e and q_t are amounts of ion adsorbed (mg/g) at equilibrium and time t (min), respectively. C_o is the initial concentration of the adsorbate in solution (mg/L), and m is the weight of the adsorbent used (g). The parameters k_1, k_2, k_{int}, and C are the adsorption rate constants of pseudo-first-

Table 4 Comparing the adsorption capacity of P(AA–MA)/Al2O3–SiO2 for cesium with those reported in literatures using other materials

Material	Media	q_e (mg/g)	References
P(AA–MA)/Al2O3–SiO2	HNO_3	16	This work
P(AM–AA–AN)/SiO_2–ZrO_2	H_2O (pH 8)	31.6	[23]
P(AM–IA)/ZrO_2	H_2O (pH 8)	43–215	[24]
Ammonium molybdophosphate–SiO_2	HNO_3	18.1	[25]
Ammonium molybdophosphate		88.2	
Fe-hexacyanoferrate	Acidic waste stimulant (pH 1.1)	16.5	[42]
Copper(II) ferrocyanide-silica		21.3	
P(AA–AN)/titanium vanadate	H_2O (pH 6)	206	[43]

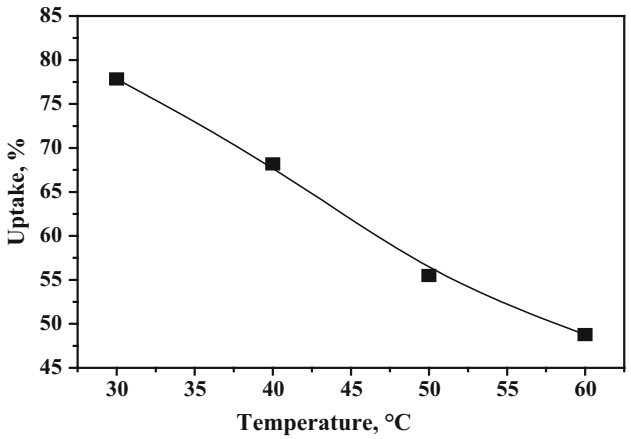

Fig. 6 Influence of temperature on the adsorption of ^{134}Cs onto P(AA–MA)SiO_2/Al_2O_3 from HNO_3

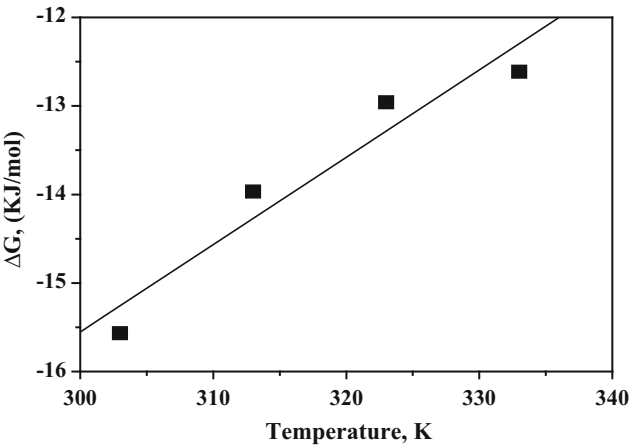

Fig. 7 Variation of free energy versus temperature for ^{134}Cs removal using P(AA–MA)SiO_2/Al_2O_3

order (min^{-1}), pseudo-second-order (g/mg min), the intraparticle diffusion rate constant (mg/g $min^{-1/2}$), and is a constant related to the thickness of the boundary layer that might be formed, respectively. In the Eq. (8) has been assumed $h = k_2 q_e^2$ where h is the initial adsorption rate (g/mg min).

A simple kinetic analysis of adsorption is the first-order equation. The values of $\log(q_e - q_t)$ were calculated from the kinetic data of Fig. 4. The plots of $\log(q_e - q_t)$ versus t for the pseudo-first-order model are given in Fig. 8 for Cs at concentration of 100–200 ppm. The k_1 values were calculated from the slope of this plot. The kinetic parameters for kinetic models and correlation coefficient (R^2) were calculated and listed in Table 6. The coefficient of determination (R^2) is ranging from 0.992 to 0.964. Moreover, the experimental q_e(exp) values do not agree with the calculated q_e. This shows that the adsorption of Cs is not compatible with the first-order reaction.

On the other hand, the plots of (t/q_t) versus t for the pseudo-second-order model given in Eq. (8) are represented at different concentration in Fig. 9. Parameters of pseudo-second-order model, q_e and k_2 values were calculated from the slope and intercept of this plot, respectively, that are presented in Table 6. The relationships are linear, and the corresponding coefficient of determination (R^2), suggested a strong relationship between the mathematical parameters and also explained that the process of sorption of ^{134}Cs follows the pseudo-second-order kinetics. From these data, it is observed that, the coefficient of determination (R^2) has a high value (0.999) and closer to unity for the pseudo-second-order kinetic model than for the pseudo-first-order kinetic model. Also, it was found the calculated sorption capacity (q_e) values, using this model, are agreement with the experimental data clarifying the matching of the experimental data to the pseudo-second-order kinetics. These results imply that the adsorption system studied follows to the pseudo-second-order kinetic model at all time intervals. It was found that the Eu, Sm, Cs, Co, Sr ions and different dyes have described the sorption kinetic process by the pseudo-second-order kinetic model as reported in [27, 43–45, 47].

The intraparticle diffusion rate was obtained from the plots q_t at versus $t^{1/2}$, as shown in Fig. 10. According to this model, plotting graphs of q_t versus $t^{1/2}$ gives a straight line. It can be assumed that the involved mechanism of the sorption process is controlled by intraparticle diffusion [45]. The values of intercept, C give an idea

Table 5 Thermodynamic parameters for sorption of ^{134}Cs onto P(AA–MA)SiO_2/Al_2O_3

Temp. (K)	Uptake (%)	ΔG (KJ/mol)	ΔH (KJ/mol)	ΔS (J/mol/K)
303	77.83431	−15.57	−45.16	98.69
313	68.17216	−13.97		
323	55.49262	−12.96		
333	48.77352	−12.61		

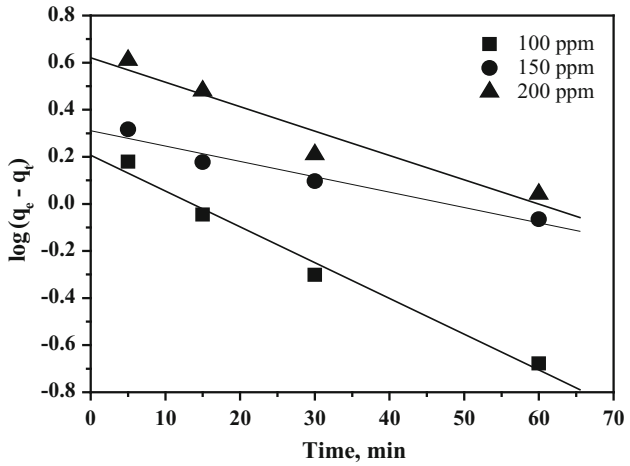

Fig. 8 Pseudo first-order model of ^{134}Cs adsorption onto P(AA–MA)SiO_2/Al_2O_3

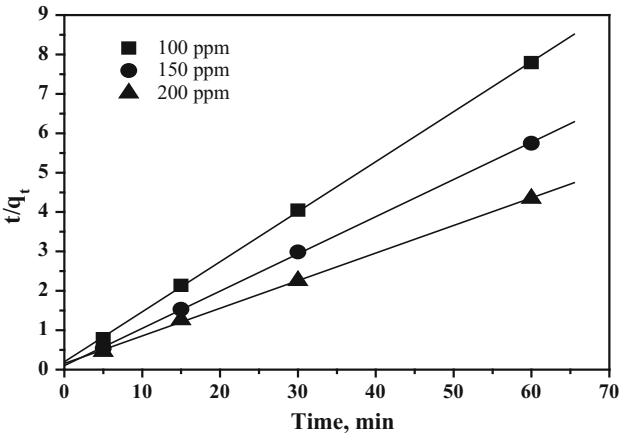

Fig. 9 Pseudo second-order model of ^{134}Cs adsorption onto P(AA–MA)SiO_2/Al_2O_3

Table 6 The calculated parameters of the kinetic models of ^{134}Cs sorbed onto P(AA–MA)SiO_2/Al_2O_3composite material

Model	Parameters	Concentration (mg/L)		
		100	150	200
Pseudo-first order	k_1 (min^{-1})	0.03	0.01	0.02
	q_e Cal. (mg/g)	1.61	2.04	4.17
	R^2	0.992	0.978	0.964
	q_e Exp. (mg/g)	7.91	11.3	14.9
Pseudo-second order	K_2 (g/mg min)	0.081	0.085	0.031
	q_e Cal. (mg/g)	7.87	10.58	14.28
	R^2	0.999	0.999	0.999
	q_e Exp. (mg/g)	7.91	11.3	14.9
Weber–Morris	Kid (mg/g $min^{0.5}$)	0.212	0.232	0.558
	C (mg/g)	6.006	8.849	9.747
	R^2	0.970	0.980	0.969

about the boundary layer thickness, i.e., the larger the intercept, the greater is the boundary layer effect. Values of C and k_{int}, the intraparticle diffusion rate constant of ^{134}Cs are given in Table 6. The present investigation is well compared with other studied that reported in [8, 27, 43, 45, 47].

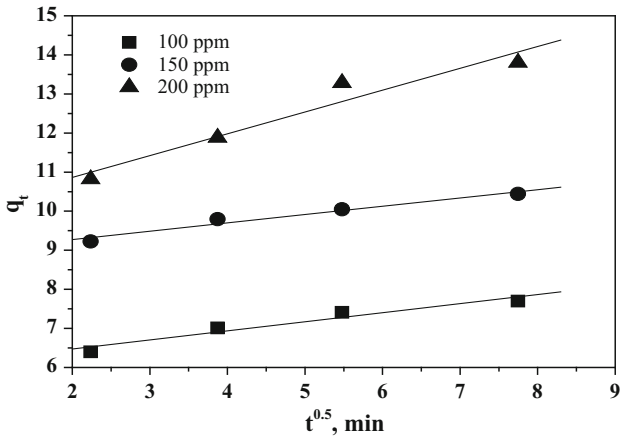

Fig. 10 Weber and Morris model of intra-particle diffusion of Cs onto P(AA–MA)SiO_2/Al_2O_3

Adsorption isotherm

Common adsorption isotherm models including Langmuir and Freundlich isotherm models were considered to fit the obtained isotherm data. Langmuir isotherm is valid for monolayer sorption onto a surface containing a finite number of identical sites. It is characterized by a decreasing slope as the concentration increases, since vacant sorption sites decrease as the sorbent becomes covered.

Langmuir sorption equation based on sorption on a homog eneous surface can be expressed as [48]:

$$\frac{1}{q_e} = \frac{1}{Q} + \frac{1}{bQC_e} \quad (10)$$

where, Q is the monolayer sorption capacity (mg/g), and b is a constant related to the free energy of sorption. By plotting of $1/q_e$ versus $1/C_e$, a straight line was obtained, as shown in Fig. 11, b and Q can be determined from the slope and the intercept, respectively. The value of b equals 0.005 L/mg and Q equals 30.9 mg/g as presented in Table 7. The essential characteristics of Langmuir isotherm can be expressed in terms of a dimensionless constant, separation factor or adsorption intensity, R_L, which is defined by:

$$R_L = \frac{1}{1 + K_L C_o} \quad (11)$$

R_L value indicates the type of isotherm to be irreversible ($R_L = 0$), favorable ($0 < R_L < 1$), linear ($R_L = 1$), or unfavorable ($R_L > 1$) [49]. The value of R_L is between 0.28 and 0.91 indicating favorable adsorption as shown in Fig. 12.

Freundlich equation is derived to model the multilayer sorption and for the sorption on heterogeneous surfaces. The logarithmic form of the Freundlich equation may be written as [48]:

$$\log q_e = \log k_L + \frac{1}{n} \log C_e \quad (12)$$

where K_F (mg/g) and n are characteristic constants related to the relative sorption capacity of the sorbent and the intensity of sorption, respectively. Plotting log q_e against log C_e gives a straight line with slope and intercept equal to 1/n and log K_F, respectively, as demonstrated in Fig. 13. The observed value of K_F of Cs^+ onto the prepared composite was found to be 0.520 mg/g and confirm a significant affinity of the Cs ions to the studied composite material. The parameter n characterizes the heterogeneity of the system. The Freundlich plot gave a slope less than 1, indicating nonlinear sorption behavior with the concentration of Cs^+ in the range studied. It can be seen from these data that the Freundlich intensity constant (n) are greater than unity for both studied ions. This has physicochemical significance with reference to the qualitative characteristics of the isotherms, as well as to the interactions between

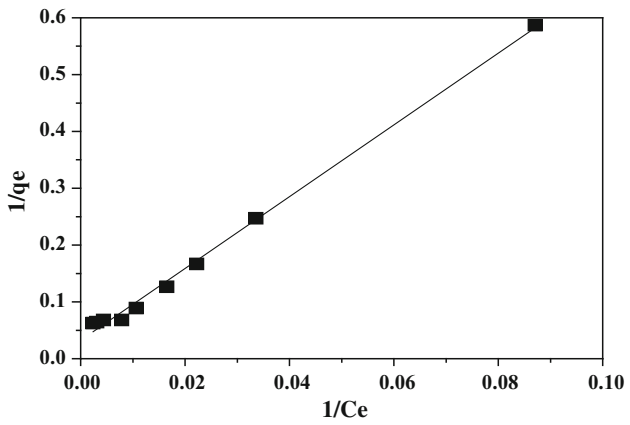

Fig. 11 Langmuir isotherm model of Cs adsorption onto P(AA–MA)SiO_2/Al_2O_3

Table 7 Langmuir and Freundlich parameters of Cs^+ adsorption on the prepared composite

Langmuir constants			Freundlich constants		
Q (mg/g)	b (L/mg)	R^2	K_F (mg/g)	n	R^2
30.90	0.0051	0.993	0.520	1.616	0.895

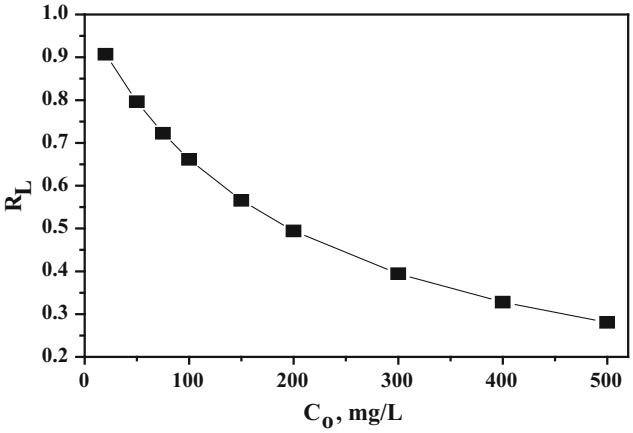

Fig. 12 Variation of adsorption intensity (R_L) with initial Cs concentration of P(AA–MA)SiO_2/Al_2O_3

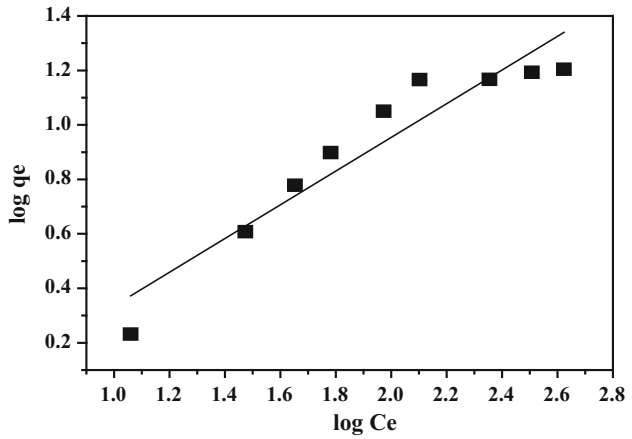

Fig. 13 Freundlich isotherm model of Cs adsorption onto P(AA–MA)SiO_2/Al_2O_3

metal ion species and composite material. In our case, $n > 1$, the composite material shows an increase tendency for sorption with increasing solid phase concentration. This should be attributed to the fact that with progressive surface coverage of adsorbent, the attractive forces between the metal ion species such as van der Waals forces, increases more rapidly than the repulsive forces, exemplified by short-range electronic or long-range Coulombic dipole repulsion, and consequently, the metal ions manifest a stronger tendency to bind to the composite material site [50]. The adsorption of Cs by the synthesized composite material obeys to Langmuir isotherm with high coefficient of determination ($R^2 > 0.99$).

Conclusion

Direct and indirect releases of large quantities of radiocesium in the environment may result in serious health and environmental problems. Therefore, isotopes of cesium should be removed from contaminated liquid before release to the environment or delivery for public use. Batch adsorption studies for the removal of ^{134}Cs from aqueous solutions have been carried out using the novel composite material. P(AA–MA)/Al2O3–SiO2 as novel composite material have been successfully synthesized by induced gamma-ray of 25 KGy. TGA showed that the composite material is high thermally stable. The adsorption equilibrium is reached at 120 min. Adsorption capacity of P(AA–MA)/Al2O3–SiO2 for Cs is 16 mg/g. The second-order kinetic model is more applicable in this study. Equilibrium isotherms have been determined and tested for different isotherm expressions and the adsorption data were successfully modeled using Langmuir and Freundlich approaches. It might be the chemisorption reaction is expected. The negative value of free energy and enthalpy means spontaneous and exothermic reaction, respectively. The preliminary investigation has given promising results for acidic radioactive liquid waste treatment containing fission product such as Cs isotopes using P(AA–MA)/Al2O3–SiO2. However, further column experiments will be needed in the upcoming work, to confirm the applicability in practice.

References

1. Parab H, Sudersanan M (2010) Water Res 44:854–860
2. Mohapatra PK, Ansari SA, Sarkar A, Bhattacharyya A, Manchanda VK (2006) Anal Chim Acta 571:308–314
3. Bykhovskii DN, Koltsova TI, Roshchinskaya EM (2009) Radiochemistry 51(2):159–164
4. Milyutin VV, Mikheev SV, Gelis VM, Kononenko OA (2009) Radiochemistry 51(3):295–297
5. El-Khouly SH, Attallah MF, Allan KF (2013) Radiochemistry 55(5):486–491
6. Kyllnen J, Hakanen M, Lindberg A, Harjula R, Vehkamki M, Lehto J (2014) Radiochim Acta 102(10):919–929
7. Park Y, Shin WS, Choi SJ (2012) J Radioanal Nucl Chem 292:837–852
8. Attallah MF, Borai EH, Allan KF (2009) Radiochemistry 51(6):622–627
9. Attallah MF, Borai EH, Hilal MA, Shehata FA, Abo-Aly MM (2011) J Hazardous Materials 195:73–81
10. Attallah MF, Borai EH, Harjula R, Paajanen A, Karesoja M, Koivula R (2011) J Mater Sci Eng B 1:736–746
11. Dai Y, Zhang A (2014) J Radioanal Nucl Chem 302:575–581
12. Kumar A, Mohapatra PK, Manchanda VK (1998) J Radioanal Nucl Chem 229:169–172
13. Raut DR, Mohapatra PK, Ansari SA, Manchanda VK (2009) Sep Sci Technol 44:3664–3678
14. Yakshin VV, Tsarenko NA, Koshcheev AM, Tananaev IG, Myasoedov BF (2012) Radiochemistry 54(1):54–58
15. VasudevaRao PR, Venkatesan KA, Rout A, Srinivasan TG, Nagarajan K (2012) Sep Sci Technol 47:204–222
16. Raut DR, Mohapatra PK, Ansari SA, Manchanda VK (2008) J Membr Sci 310:229–236
17. Kandwal P, Mohapatra PK, Ansari SA, Manchanda VK (2010) Radiochim Acta 98:493–498
18. Raut DR, Mohapatra PK, Choudhary MK, Nayak SK (2013) J Membr Sci 429:197–205
19. Raject P, Matel L, Orechovska J, Sucha J, Vovak I (1996) J Radioanal Nucl Chem 208(2):477–486
20. Guin R, Das SK, Saga SK (2002) Radiochim Acta 90:53–56
21. Granados F, Bertin V, Bulbulian S, Solache-Rios M (2006) Appl Radiat Isot 64:291–297
22. Raut DR, Mohapatra PK, Wattal PK, Manchanda VK (2012) J Radioanal Nucl Chem 292:661–666
23. Allan KF, Holiel M, Sanad WA (2014) Radiochemistry 56(3): 267–274
24. Hamoud MA, Allan KF, Sanad WA, El-Hamouly SH, Ayoub RR (2014) J Radioanal Nucl Chem 302:169–178
25. Ingale SV, Ram R, Sastry PU, Wagh PB, Kumar R, Niranjan R, Phapale SB, Tewari R, Dash A, Gupta SC (2014) J Radioanal Nucl Chem 301:409–415
26. Toropov AS, Satayeva AR, Mikhalovsky S, Cundy AB (2014) Radiochim Acta 102(10):911–917
27. Hamed MM, Attallah MF, Metwally SS (2014) Radiochim Acta 102(11):1017–1024
28. Kandwal P, Mohapatra PK (2014) Radiochim Acta 102(9): 831–838
29. Trantera TJ, Herbsta RS, Todda TA, Olsona AL, Eldredg HB (2002) Adv Environ Res 6:107
30. Hassan NM, Adu-Wusu K, Marra JC (2004) J Radioanal Nucl Chem 262(3):579–586
31. Mrad O, Abdul-Hadi A, Arsan H (2011) J Radioanal Nucl Chem 287:177–183
32. Klavetter EA, Brown NE, Trudell DE, Anthony RG, Gu D and Thibaud-Erkey C (1994) Ion-exchange performance of crystalline silicotitanates for cesium removal from Hanford tank waste simulants. In: Proceedings of waste management, vol 1. Tucson, p 709
33. Anthony RG, Dosch RG, Gu D, Philip CV (1994) IEC Res 33(11):2702–2705
34. Zheng Z, Gu D, Anthony RG, Klavetter EA (1995) IEC Res 34(6):2142–2147
35. Todd TA, Romanovskiy VN (2005) Radiochemistry 47(4): 398–402
36. Ali IM, El-Zahhar AA, Zakaria ES (2003) In: 7th Arab international conference on polymer science and technology part (1), p. 363

37. Clearfield A (1982) Inorganic ion exchang material. CRC Press, Boca Raton
38. Allan KF, Siyam T and Sanad WA (2001) 6th Arab international conference on polymer science and technology part (2), p 21
39. Hassan HS (2004) Ph.D. Thesis, Faculty of Science. Mansoura University, Egypt
40. Haberko K, Pampuch R (1983) Ceram Inter 4(1):148
41. Chang MY, Juang RS (2004) J Colloid Interface Sci 278:18–25
42. Sangvanich T, Sukwarotwat V, Wiacek RJ, Grudzien RM, Fryxell GE, Addleman RS, Timchalk C, Yantasee W (2010) J Hazard Mater 182(1–3):225–231
43. El-Gammal B, Ibrahim GM, Allan KF, El-Naggar IM (2009) J Appl Polym Sci 113:3405–3416
44. Attallah MF, Ahmed IM, Hamed MM (2013) Environ Sci Pollut Res 20:1106–1116
45. Hassan HS, Attallah MF, Yakout SM (2010) J Radioanal Nucl Chem 286:17–26
46. Hamed MM (2014) J Radioanal Nucl Chem 302:303–313
47. Attallah MF, Borai EH, Shady SA (2014) J Radioanal Nucl Chem 299:1927–1933
48. Dada AO, Olalekan AP, Olatunya AM, Dada O (2012) J Appl Chem 3(1):38–45
49. Metwally SS, Hassan MA, Aglan RF (2014) J Environ Chem Eng 1(3):252–259
50. Mohan D, Singh KP (2002) Water Res 36:2304–2318